Supporting Information

Alkaline-earth Ions Stabilized Sub-nano Platinum Tin Clusters for Propane Dehydrogenation

Zhenpu Lu,[ab] Ran Luo,[ac] Sai Chen,[ab] Donglong Fu,[ab] Guodong Sun,[abc] Zhi-Jian Zhao,[abd] Chunlei Pei,*[ab] and Jinlong Gong*[abcd]

[a.] *Key Laboratory for Green Chemical Technology of Ministry of Education, School of Chemical Engineering and Technology, Tianjin University*

[b.] *Collaborative Innovation Center of Chemical Science and Engineering, Tianjin 300072, China*

[c.] *Joint School of National University of Singapore and Tianjin University, International Campus of Tianjin University, Binhai New City, Fuzhou 350207, China*

[d.] *Haihe Laboratory of Sustainable Chemical Transformations, Tianjin 300192*

Experimental method

Catalyst preparation.

All the catalysts were prepared by incipient wetness co-impregnation method. $H_2PtCl_6 \cdot 6H_2O$ (Chemart (Tianjin) Chemical Technology Co., Ltd, 99.9%) and $SnCl_4 \cdot 5H_2O$ (Aladdin (China) Chemical Co., Ltd, 98.0%) were mixed and used as precursors and γ-Al_2O_3(Sinopharm Chemical Reagent Co., Ltd, 98.0%) was used as support. After impregnation, the catalysts were left to stand in the atmosphere overnight, then dried in flowing air at 353 K for 12 h, and then calcined at 873 K for 2 h.

Characterization method.

Transmission electron microscope (TEM) images were taken using a JEOL JEM 2100F system at an accelerating voltage of 200 kV equipped with a field emission gun. The sample was firstly reduced at 873 K for 1 h in a stream of 18 vol% H_2/N_2. Then, the sample powder was dispersed in deionized water by ultrasonic and supported on a copper grid coated with an ultrathin holey carbon film.

High-angle annular dark-field scanning transmission electron microscopy (HAADF-STEM) images were collected using a JEOL JEM 2100F system at an accelerating voltage of 200 kV equipped with a field emission gun. The sample was first reduced at 873 K for 1 h in a stream of 18 vol% H_2/N_2. Then, the sample powder was dispersed in deionized water by ultrasonic and deposited on a copper grid coated with an ultrathin holey carbon film.

The in-situ diffuse reflectance infrared Fourier-transform spectroscopy (DRIFTS) experiments were performed on a Thermo Scientific Nicolet IS50 spectrometer, equipped with a Harrick Scientific DRIFTS cell fitted with ZnSe windows and a mercury–cadmium–telluride (MCT) detector cooled by liquid N_2. The catalysts were heated from ambient temperature to 873 K at a rate of 10 K/min and retained at 873 K in a flow rate of 50 mL min^{-1} of 20 vol% H_2 /Ar. Then, the catalysts were cooled down to 303 K and the backgrounds (8 cm^{-1} resolution, 64 scans) were collected after Ar purging in a flow rate of 20 mL min^{-1} for at least 1 h. With the addition of a flow of 3 mL min^{-1} of CO, the adsorption of CO molecules on the surface of the catalysts continued for 30 min. After that, the DRIFTS spectra were recorded till no visible change in the absorption band intensities under Ar purging.

Quasi in situ XPS was performed was performed on a Thermo Fischer ESCALAB Xi+ photoelectron spectrometer with monochromated X-ray irradiation Al Kα (hv = 1486.7 eV) and a 180°double focusing hemispherical analyzer with a six-channel detector. The pretreatment of samples was performed in a UHV-connected high-pressure gas cell. Samples were heated in 10% H_2/Ar flow (30 mL/min, 1 bar) at 600 °C for 60 min for reduction. The photoelectron spectra were recorded after UHV transfer of the samples to the analyzer chamber without contact with the atmosphere.

Catalytic test.

Catalytic tests were performed in a quartz fixed-bed reactor with 8 mm inner diameter and 24 cm length at atmosphere pressure. Typically, A volume of 100 mg of the calcined catalyst with particle size of 40–60 mesh was packed inside the quartz tubular reactor. The sample was first heated to 873 K at a rate of 10 K/min and retained at 873 K for 1 h in flowing 18 vol% H_2/N_2. Afterward, a mixture of C_3H_8, H_2, and N_2 (8:8:34 vol%) was fed at a rate of 50 mL min^{-1}. The weight hourly velocity (WHSV) of propane was around 8.25 h^{-1}. The gas products were analyzed by an online GC (2060) equipped with a flame ionization detector (Chromosorb 102 column) and a thermal conductivity detector (Al_2O_3 Plot column). The propane conversion and selectivity to propylene were calculated from Eq. (1) and Eq. (2), respectively:

$$Con(\%) = 100 \times \left(\left[F_{C3H8}\right]_{\text{inlet}} - \left[F_{C3H8}\right]_{\text{outlet}}\right)/\left[F_{C3H8}\right]_{\text{inlet}} \quad (1)$$

$$Sel(\%) = 100 \times \left[F_{C3H6}\right]_{\text{outlet}}/\left(\left[F_{C3H8}\right]_{\text{inlet}} - \left[F_{C3H8}\right]_{\text{outlet}}\right) \quad (2)$$

Where F_{C3H8} and F_{C3H8} means mole flow rate of propane and propylene. A firstorder deactivation model was used to evaluate the catalyst stability:

$$k_d = \left(ln\left[\left(1 - X_{\text{final}}\right)/X_{\text{final}}\right] - ln\left[\left(1 - X_{\text{initial}}\right)/X_{\text{intial}}\right]\right)/t \quad (3)$$

where X_{intial} and X_{final} , respectively, represent the conversion measured at the initial and final period of an experiment, and t represents the reaction time (h), k_d is the deactivation rate constant (h^{-1}). High k_d value means rapid deactivation, that is, low stability. The mean catalyst life represents the time required for rates to decrease by e^{-1}, and is estimated with the reciprocal of the deactivation rate constants.

For the regeneration of the catalysts, using 1% O_2 as a mild oxidant at 773 K followed by reduction at 873 K. Typically, after four hours' propane dehydrogenation reaction,the catalyst underwent a cooling process to reach a temperature of 773K while being shielded by a nitrogen atmosphere (at a flow rate of 34 ml/min). Subsequently, a 1% O_2/N_2 mixture was introduced and allowed to react for 20 minutes to remove the coke. The gas stream was then switched to nitrogen for a duration of 5 minutes to eliminate the oxidizing gas. Following this, the catalyst was introduced and gradually heated to 873K under a 20% H_2/N_2 (42 ml/min) and maintained for 1 hour to the next propane dehydrogenation reaction.

Calculation methods.

All the spin-polarized DFT calculation was performed in the plane-wave pseudopotential method based on the GGA-PBE exchange-correlation functional,[1] which is implemented by Vienna *ab initio* simulation package (VASP, 5.4.4 version[2]).

The valence wave functions were expanded by plane wave with a cutoff energy of 400 eV. We established the model of SnO_x and SnO_x with CaO_x on the (001) surface of gamma aluminum. The vaccum layer is set as 15 Å. The Brillouin zone was sampled using 3x3x1 k points mesh for geometry optimization. All the structures were optimized until the force on each atom was less than 0.02 eV $Å^{-1}$.

The vacancy formation energies were calculated according to following equation, we used H_2(g) and H_2O(g) to avoid the overbinding problem of caluclation of O_2(g) molecule.

$$H_2(g) + SnO_x \rightarrow H_2O(g) + SnO_{x-1}$$

Moreover, all clusters migration barriers calculations were performed by using the climbing-image nudged elastic band method (NEB)[3] and further improved by dimer method[4]. The activation barrier E_a was calculated based on following equation:

$$\Delta E_a = E_{TS} - E_{IS}$$

Table S1. Summary of PDH performance data for various reported Pt-containing catalysts

NO.	Catalysts	Temperature (K)	Loading of Pt（wt%）	Propane WHSV (h-1)	gas compositions	Initial Conversion Rate	Final Conversion Rate	C_3H_6 formation rate mol/(gPt*h)	Reaction durations (h)	Deactivation rate（h^{-1}）	Mean catalyst life (h)	Ref.
1	Pt-Sn/$MgAl_2O_4$	848	1.00%	14.70	C_3H_8:H_2=1:0.8, Ar balance atmospheric pressure	33.00%	29.00%	10.91	3.3	0.0567	17.6	[5]
2	Pt-Sn/ZSM-5	863	0.50%	3.00	C_3H_8:H_2=4:1 0.1 MPa	33.10%	26.30%	2.55	6	0.0545	18.4	[6]
3	Pt-Sn/γ-Al2O3	863	0.50%	3.00	C_3H_8:H_2=4:1 0.1 MPa	29.40%	22.70%	3.61	6	0.0582	17.2	
4	Pt-Sn / mesoporous Al_2O_3	863	0.50%	3.00	C_3H_8:H_2=4:1 0.1 MPa	29.80%	24.60%	3.66	6	0.0439	22.8	
5	PtSn/Al_2O_3 sheet	863	0.50%	9.40	C_3H_8:H_2:N_2=1:1.25:4 atmospheric pressure	48.70%	44.60%	20.62	6	0.0069	145.6	[7]
6	2Pt-0.6Sn/γ-Al_2O_3	813	2.00%	3.53	C_3H_8:H_2:N_2=3:1:21 atmospheric pressure	42.90%	39.20%	1.68	24	0.0191	52.3	[8]
7	2Pt-1.2Sn/-Al_2O_3	813	2.00%	3.53	C_3H_8:H_2:N_2=3:1:21 atmospheric	43.50%	41.40%	1.73	8	0.0107	93.1	

					pressure							
8	2Pt-2.4Sn/γ-Al_2O_3	813	2.00%	3.53	C_3H_8:H_2:N_2=3:1:21 atmospheric pressure	42.80%	41.70%	1.71	8	0.0056	177.4	
9	Pt-Sn-5/$MgAl_2O_4$	853	0.42%	2.35	C_3H_8:H_2:He=1:1:8 atmospheric pressure	45.00%	37.60%	5.71	90	0.0034	294.2	[9]
10	Pt-Sn-6/$MgAl_2O_4$	853	0.39%	2.35	C_3H_8:H_2:He=1:1:8 atmospheric pressure	45.00%	38.90%	6.15	90	0.0028	358.8	
11	Pt-Sn/Al_2O_3	792	0.35%	3.50	C_3H_8:H_2:N_2=3:1:6 0.1MPa	31.00%	20.00%	6.69	10	0.0586	17.1	[10]
12	PtSnNa/Al-SBA-15	863	0.50%	3.00	C_3H_8:H_2=4:1 0.1MPa	27.50%	12.60%	3.53	40	0.0242	41.4	[11]
13	PtSn/15MAF	863	0.46%	3.00	C_3H_8:H_2=4:1 atmospheric pressure	24.70%	23.50%	3.39	7	0.0094	106.7	[12]
14	PtSn/$MgAl_2O_4$	823	0.50%	47.14	C_3H_8:H_2=1:1 0.08MPa	12.00%	11.00%	23.66	3	0.0328	30.5	[13]
15	Pt/Mg(Sn)(Al)O@Al_2O_3	823	0.50%	14	C_3H_8:H_2:Ar=1:0.5:2 atmospheric pressure	48.3%	43%	26.55	240	0.004	250	[14]
16	Pt0.5-Ge1.5/$A_{l2}O_3$-CaO	873	0.5%	23.6	C_3H_8:H_2:N_2:Ar=2:1:16.78:0.22	21%	17%	22.16	24	0.011	90	[15]

					atmospheric pressure							
17	0.04Pt-0.36Zn-DeAlBEA	823	0.04%	216	C_3H_8:He=1:3 atmospheric pressure	18.2%	17.5%	125.8	160	0.004	250	[16]
18	K-PtSn@MFI-600H2-22h	823	0.4%	118.1	C_3H_8:N_2=5:16 atmospheric pressure	20%	17%	129.8	15	0.003	333	[17]
19	K-PtSn@MFI-600H2-22h	873	0.4%	29.5	C_3H_8:N_2=5:16 atmospheric pressure	38.7%	31.9%	62.85	70	0.013	77	[17]
20	K-PtSn@MFI	873	0.42%	1.8	C_3H_8:N_2=5:16 atmospheric pressure	20%	17%	6.27	68	0.014	71	[18]

Table S2. Pulse chemisorption of hydrogen on $PtSn3/Al_2O_3$ compared with $PtSn3Ca5/Al_2O_3$

Catalyst	H_2 uptake ($ml/g_{catalyst}$)
$PtSn3/Al_2O_3$	0.2344
$PtSn3Ca5/Al_2O_3$	0.3023

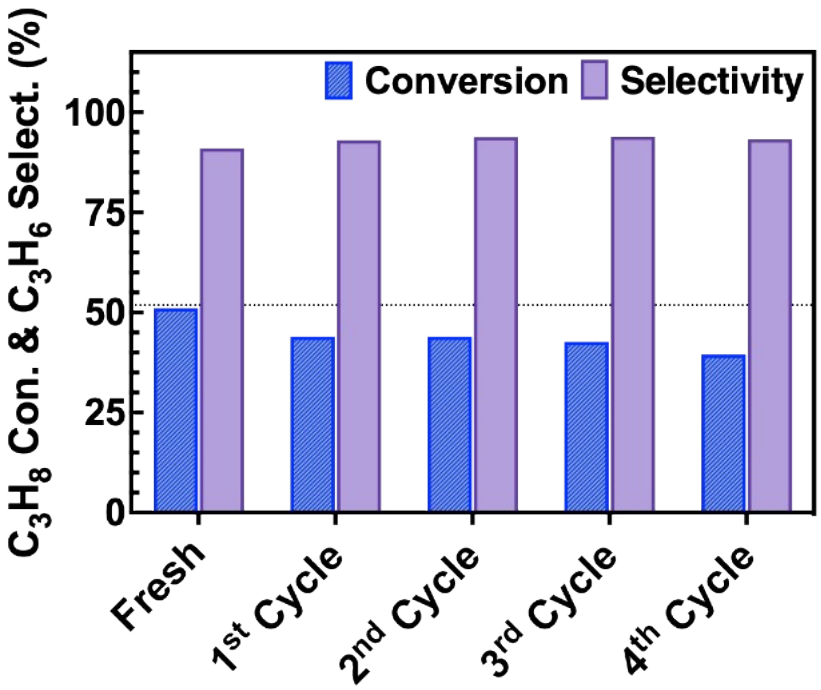

Figure S1. Catalytic performances on the PtSn3/Al_2O_3 catalyst for each of the five dehydrogenation cycles. Catalytic conditions: atmospheric pressure, C_3H_8/H_2 = 1/1, with balance N_2 for total flow rate of 50 mL/min, WHSV of propane = 8.25 h^{-1} and 100 mg of sample.

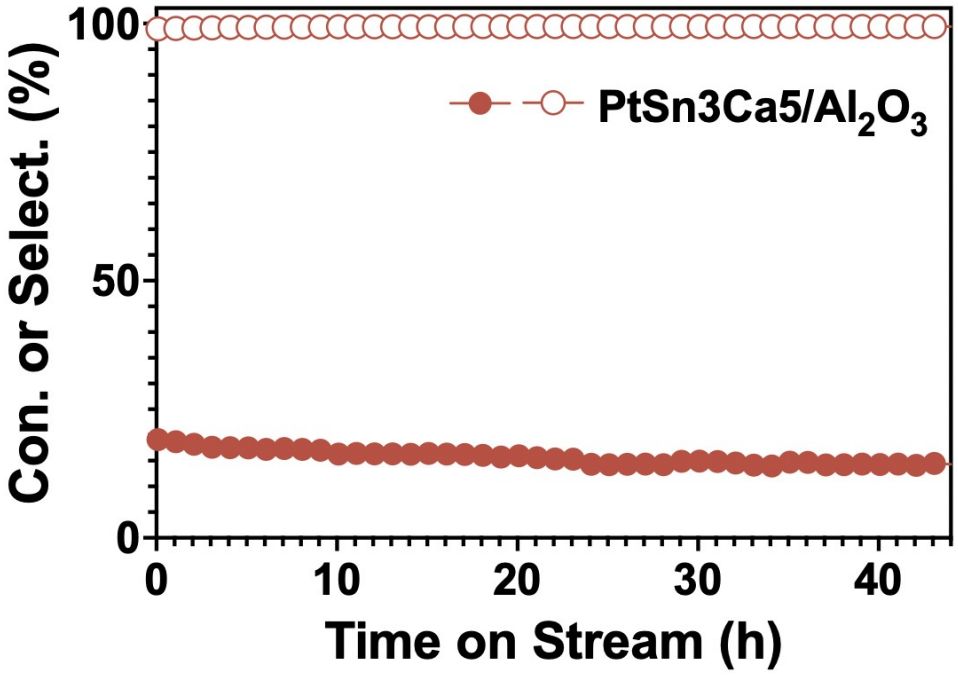

Figure S2. Propane dehydrogenation with $PtSn3Ca5/Al_2O_3$ catalyst under a WHSV of ~100 h^{-1}. The catalyst was reduced by 14%H_2/N_2 at 600 °C for 1 h and then cool to 550 °C in 14%H_2/N_2 flow, before changing the atmosphere to feed gas. Reaction conditions: 30 mg catalyst, 25 mL/min of propane and 12.5 mL/min H_2 as feed gas, 550 °C.

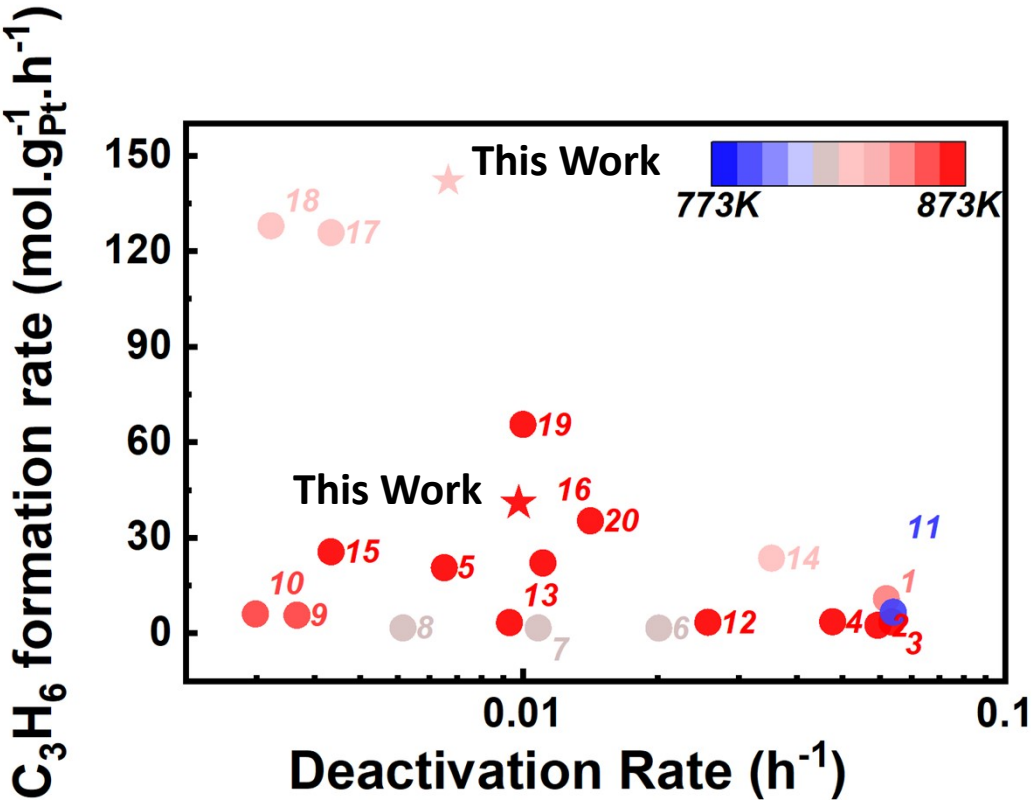

Figure S3. Productivity of C_3H_6 versus deactivation rate for the state of art catalysts described in this work and literatures (Table S1). The pentagonal points are the catalysts reported in this paper under different WHSV.

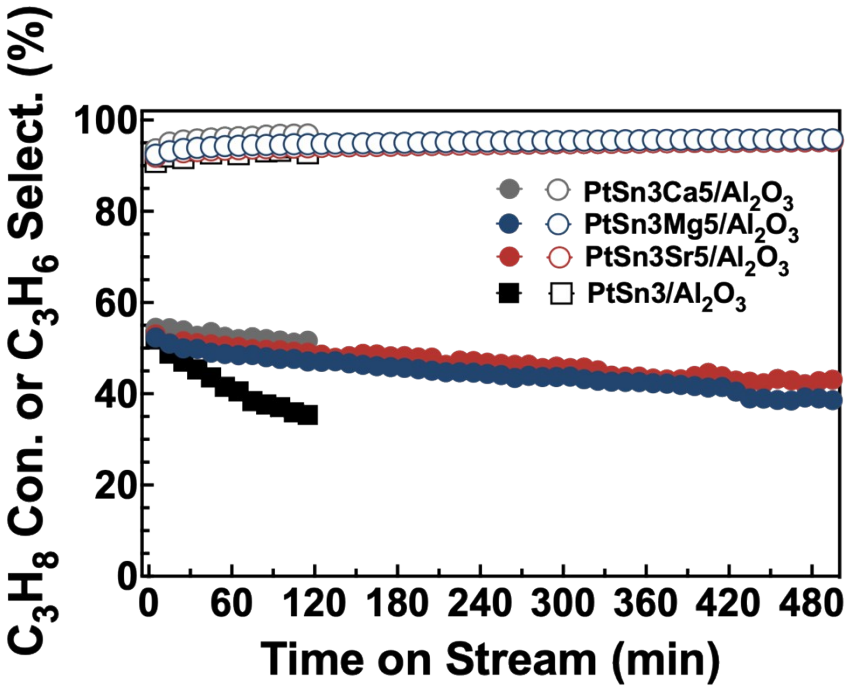

Figure S4. Propane conversion and propylene selectivity as a function of reaction time over the prepared PtSn3/Al_2O_3, PtSn3Mg5/Al_2O_3 and PtSn3Sr5/Al_2O_3 at 873 K. Catalytic conditions: atmospheric pressure, C_3H_8/H_2 = 1/1, with balance N_2 for a total flow rate of 50 mL/min, WHSV of propane = 8.25 h^{-1}, and 100 mg of sample.

PtSn3Ca5/Al_2O_3 shows best catalytic stability since the lowest k_d was obtained. (k_d of about 0.040 h^{-1}, 0.044 h^{-1} and 0.059 h^{-1} for PtSn3Ca5/Al_2O_3, PtSn3Sr5/Al_2O_3 and PtSn3Mg5/Al_2O_3, respectively).

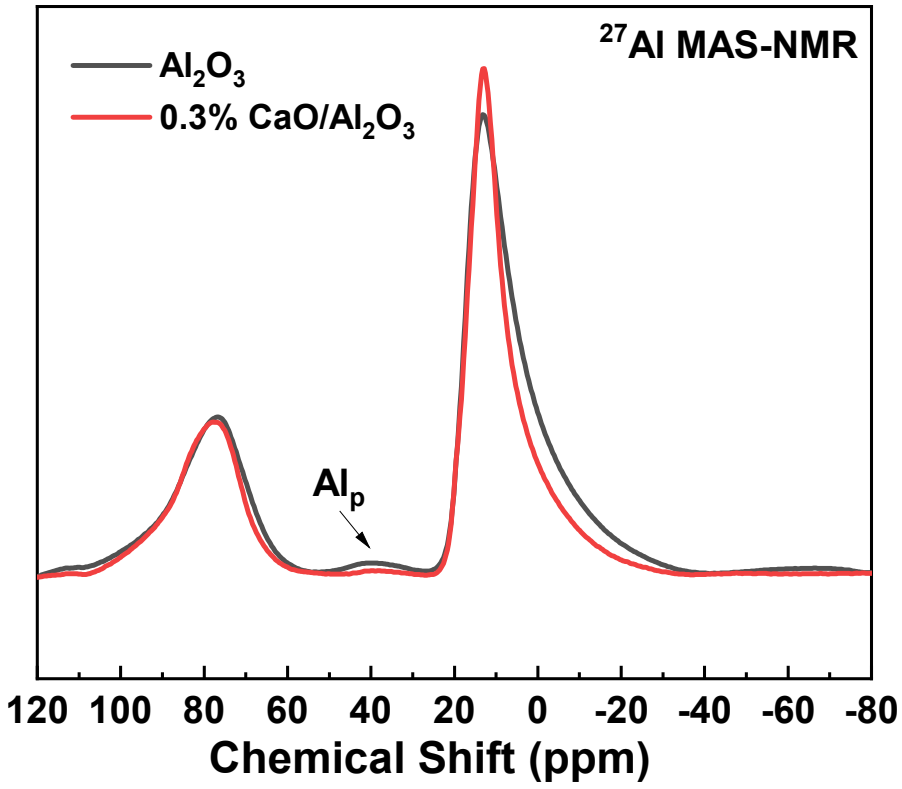

Figure S5. The 27Al MAS-NMR spectra of Al_2O_3 (black) and 0.3 wt% CaO/Al_2O_3 (red) (both samples were calcined at 873 K before NMR measurements).

Figure S5 shows the high-resolution ^{27}Al solid state MAS-NMR spectra of the Al_2O_3 and 0.3 wt.% CaO/Al_2O_3 samples. Three characteristic ^{27}Al NMR features of Al_2O_3 at 13 ppm, 39 ppm and 76 ppm represent octahedral coordination (Al^{3+}_{octa}), penta coordination (Al^{3+}_{penta}) and tetrahedral coordination of Al^{3+} ions (Al^{3+}_{tetra}), respectively.[19] After loading CaO onto the Al_2O_3 and calcining at 873 K, the number of Al^{3+}_{penta} was significantly reduced, as evidenced by the decrease in the intensity of the NMR peak at 39 ppm. This result strongly suggests that Ca atoms bind to the Al^{3+}_{penta} sites on the Al_2O_3 surface via oxygen bridges, thereby coordination saturating these sites, which is similar to the binding behavior of platinum atoms with Al_2O_3[20,21].

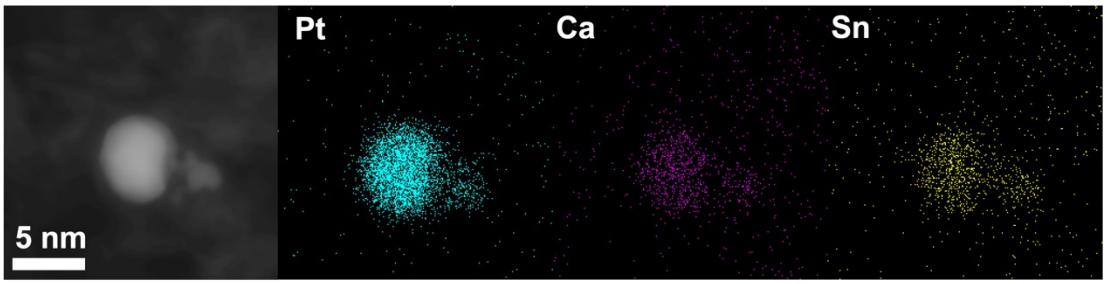

Figure S6. EDS mapping of 3% PtSn3Ca5/Al_2O_3.

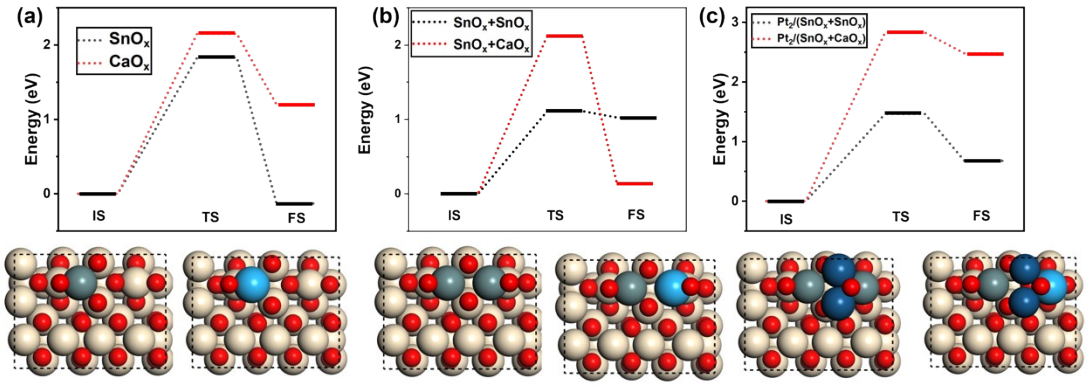

Figure S7. Potential energy diagram of SnO_x migration.

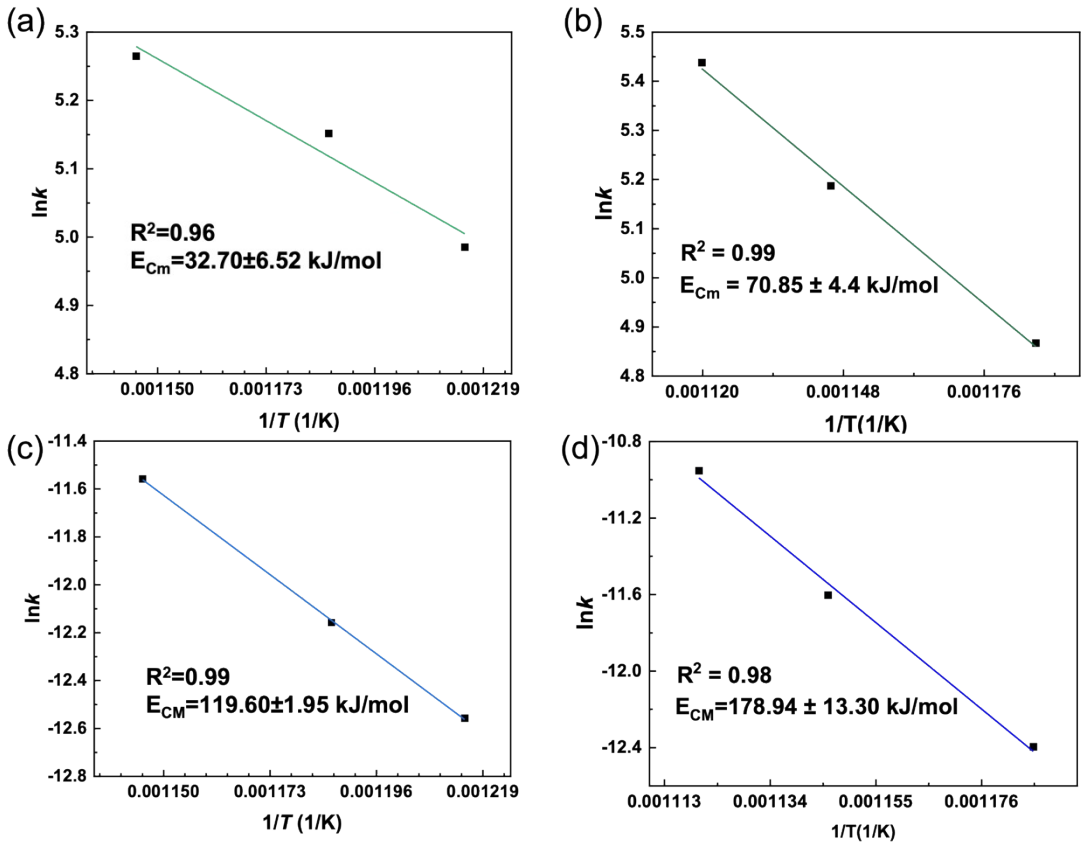

Figure S8. Activation energy for monolayer coking (E_{Cm}) of (a) $PtSn3/Al_2O_3$ and (b) $PtSn3Ca5/Al_2O_3$; and multilayer coking (E_{CM}) (c) $PtSn3/Al_2O_3$ and (d) $PtSn3Ca5/Al_2O_3$

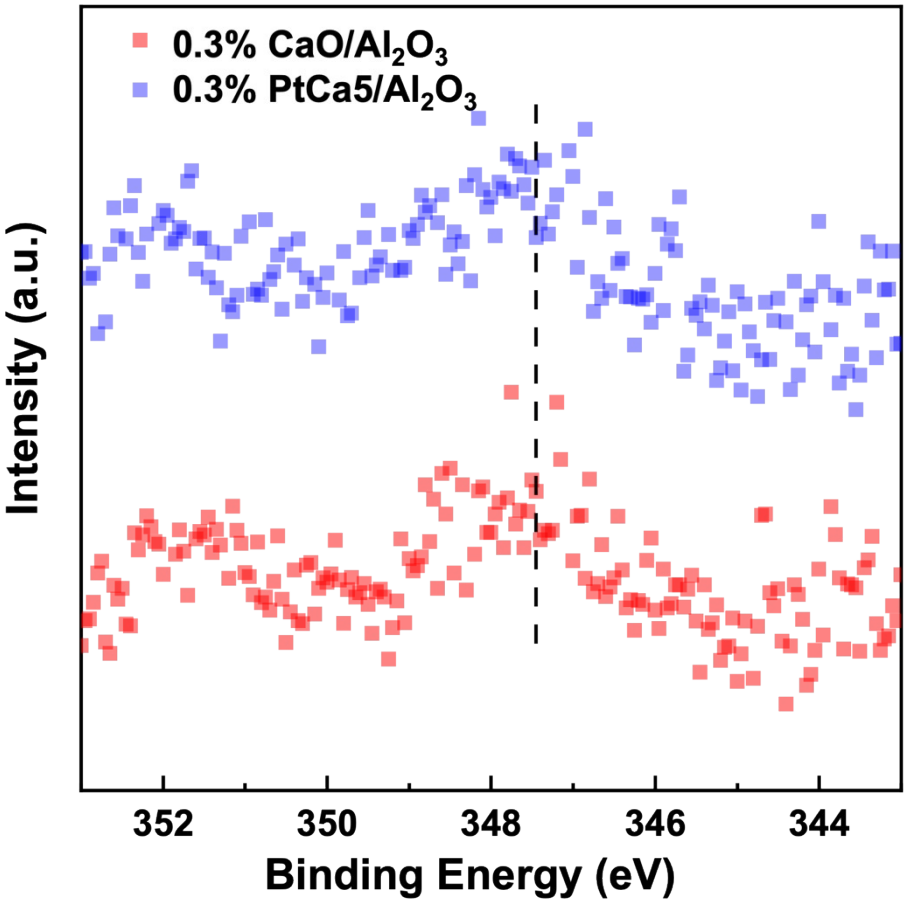

Figure S9. XPS spectra of Ca 2p in 0.3% CaO/Al_2O_3 and 0.3% $PtCa5/Al_2O_3$

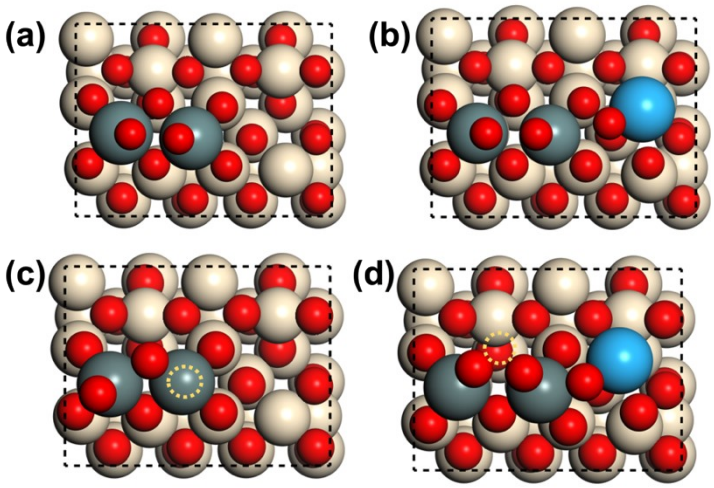

Figure S10. Atomic models of (a)SnO_x/Al_2O_3 and (b) SnO_x/Al_2O_3 with CaO_x; Defective srtructures of (c)SnO_x/Al_2O_3 and (d)SnO_x/Al_2O_3 with CaO_x with oxygen vacancies that possess most negative formation energies (yellow circles denotes the positions of vacancies). Yellow spheres denote Al atoms; red spheres denote oxygen atoms; green spheres denote Sn atoms while Ca atom is in bule.

We constructed atomic models of SnO_x dimer which is constituted by two Sn-O octahedrons (Figure S7a). Similar coordination pattern is also shown in SnO_2. Further, as shown in Figure S7b, a Ca-O tetrahedron, which is the unit structure in CaO_2, is added into the model to explore the function of Ca in our catalyst. We conducted oxygen vacancy formation energy calculations in the models and results are shown in Figure 3d. It should be noted that we chose H_2(g) and H_2O(g) as reference for the oxygen vacancy formation calculation to simulate the real reduction process by H_2(g). The chosen of O_2(g) as a reference traditionally would yield a higher oxygen vacancy formation energy, but the O_2 molecular energy prediction problem (over-binding problem) would occur for the GGA level functional[22]. For the three kinds of oxygen species in SnO_x, Sn=O, Sn-O-Sn and Sn-O-Al, only the formation energy Sn=O remains unchanged with CaOx, while formation energies of Sn-O-Sn and Sn-O-Al decrease obviously after the addition of CaO_x. Hence, Ca promotes the reducibility of SnO_x. Besides, in SnOx, formation of vacancy would not lead to obvious relaxation of structure (Figure S7c), whiles in SnO_x with CaO_x, formation of vacancy would generally lead to formation of Sn-O-Ca (Figure S7d), which proves the reduction process is also an aggregation process of SnO_x and CaO_x.

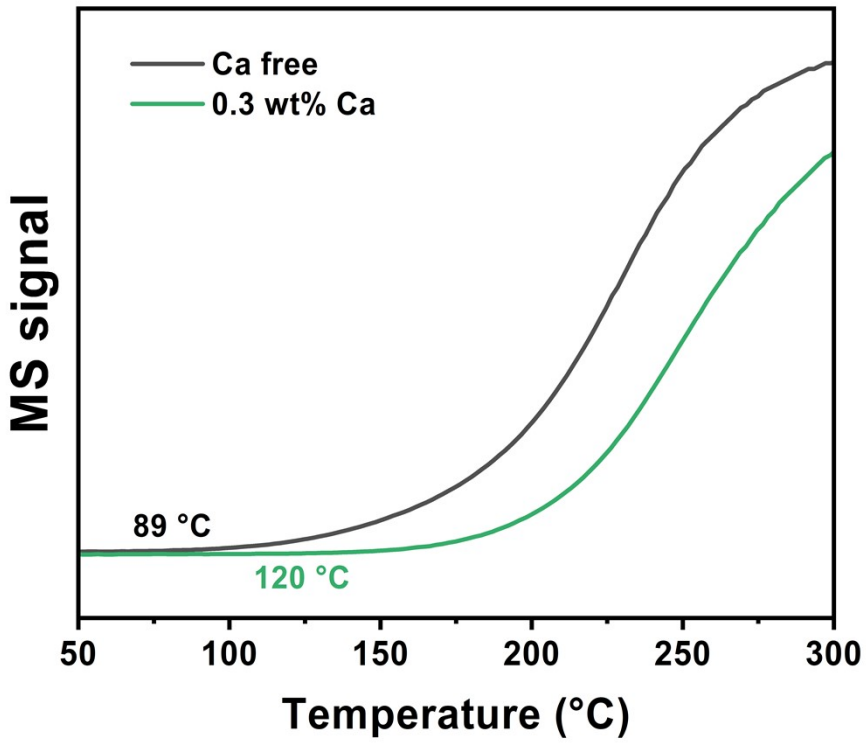

Figure S11. Signals of C_3H_7D during C_3H_8-D_2 TPSR over PtSn3/Al_2O_3 (Ca free) and PtSn3Ca5/Al_2O_3 (0.3 wt% Ca).

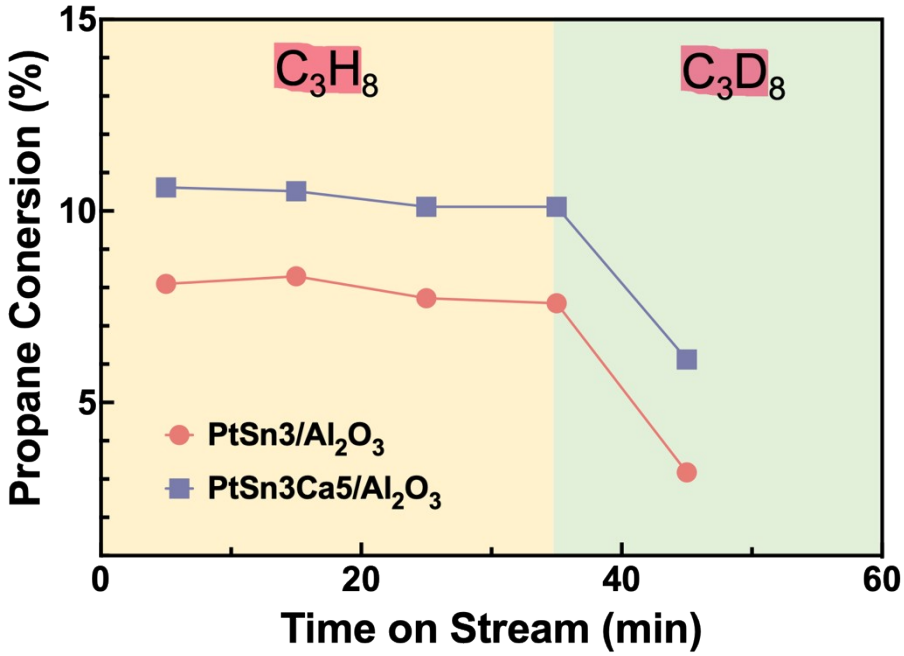

Figure S12. KIEs of propane dehydrogenation on of $PtSn3/Al_2O_3$ and $PtSn3Ca5/Al_2O_3$

The rate determining step (RDS) determines the KIE and the reaction order of H_2, thus the difference in KIE would imply the reaction order of H_2. Generally, either the First C-H bond cleavage or the Second C-H bond cleavage is considered to be RDS (Table S3). The reaction order with respect to H_2 varies from 0 to -0.5 when the presumed RDS shifts from the first C−H bond activation to the second C−H bond activation while the H surface coverage is rather low[23].

Table S3. Reaction Pathway of Propane Dehydrogenation

	Elementary reaction	Description
(I)	$C_3H_8 + * \leftrightarrow C_3H_8*$	Adsorption of propane
(II)	$C_3H_8 * + * \leftrightarrow C_3H_7* + H*$	First C-H bond cleavage
(III)	$C_3H_7* + * \leftrightarrow C_3H_6* + H*$	Second C-H bond cleavage
(IV)	$C_3H_6* \leftrightarrow C_3H_6 + *$	Desorption of propylene
(V)	$2H* \leftrightarrow H_2 + 2*$	Desorption of hydrogen

Besides, it was demonstrated by varies groups[23,24] that the kinetic isotope effect (KIE) strongly correlates to the rate determine step (RDS) of the PDH reaction. The replacement of H with D at the position of C–H activation decreases the rate of reactions limited by C–H bond cleavage, leading to kinetic isotope effect.

The rate of propane dehydrogenation is proportional to

$$r \propto K_i k_{i'}$$

and the kinetic isotope effect (KIE) which is defined as the ratio of PDH reaction rates equals to

$$KIE = \frac{r_H}{r_D} = \frac{K_{i,H} k_{i',H}}{K_{i,D} k_{i',D}}$$

In which r_H or r_D is the PDH reaction rates wish C_3H_8 or C_3D_8, respectively. $K_{i,H}$ and $K_{i,D}$ are the chemical equilibrium constant of step i with C_3H_8 or C_3D_8, respectively. $k_{i',H}$ and $k_{i',D}$ are rate constant of step i' with C_3H_8 or C_3D_8, respectively.

Assuming that first C-H cleavage is the rate determine step, then the kinetic isotope effect (KIE) which is defined as the ratio of PDH reaction rates equals to

$$KIE = \left(\frac{K_{I,\ C_3H_8}}{K_{I,\ C_3D_8}}\right)\left(\frac{k_{II,\ C_3H_8}}{k_{II,\ C_3D_8}}\right)$$

Each parenthesis in above equation is examined separately as follows.

$$\frac{K_{I,\ C_3H_8}}{K_{I,\ C_3D_8}} = \frac{\dfrac{Q_{C_3H_8*}}{Q_{C_3H_8} Q*}}{\dfrac{Q_{C_3D_8*}}{Q_{C_3D_8} Q*}}$$

$$\frac{k_{II,\ C_3H_8}}{k_{II,C_3D_8}} = \frac{\dfrac{Q_{\overset{\Xi}{C_3H_7}*H*}}{Q_{C_3H_8} * Q*}}{\dfrac{Q_{\overset{\Xi}{C_3D_7}*D*}}{Q_{C_3D_8} * Q*}}$$

Then,

$$KIE = \frac{Q_{\overset{\Xi}{C_3H_7}*H*} Q_{C_3D_8}}{Q_{\overset{\Xi}{C_3D_7}*D*} Q_{C_3H_8}}$$

The contributions to KIE come from four different parts: translational (Q_{trans}), rotational (Q_{rot}), vibrational (Q_{vib}), and electronic partition functions (Q_{elec}). Each ratio of partition functions is evaluated as follows.[24]

$$Q_{trans} = \frac{(2\pi m k_b T)^{3/2} V}{h^3} \propto (mT)^{3/2}$$

$$Q_{rot} = \frac{8\pi^2}{\sigma h^3}(2\pi k_b T)^{3/2}(I_x I_y I_z)^{1/2} \propto T^{3/2}(I_x I_y I_z)^{1/2}$$

$$Q_{vib} = \sum_{v=0}^{\infty} e^{-v\theta_v/T} \approx \frac{1}{1-e^{-\theta_v/T}}, \text{ where } \theta_v = \frac{h}{2\pi k_b}\sqrt{\frac{k}{\mu}}$$

$$Q_{\text{elec}} = g_0 + g_1 e^{-\varepsilon_1/k_b T} + g_2 e^{-\varepsilon_2/k_b T} + \cdots \approx g_0 = e^{-\varepsilon_0/RT}$$

In which the h represents Planck's constant; I_x, I_y,$and\ I_z$ represent moments of inertia; k denotes force constant; k_b is Boltzmann's constant; m signifies the mass of molecules or atoms; T denotes temperature in Kelvin; V stands for volume; μ=$m_1m_2/(m_1+m_2)$ represents the reduced mass; ε_0 signifies the zero-point energy; σ denotes the symmetry number; and $\theta_v$indicates the characteristic temperature for vibration in Kelvin.

(1) Translational partition function contribution:

The C_3H_7*H* and C_3D_7*D* adsorbed species have zero translational degrees of freedom, and the reduce masses of C_3H_7*H* and C_3D_7*D* adsorbed species are approximately the same. Therefore, $(\frac{Q_{C_3H_7^{\Xi}*H*}}{Q_{C_3D_7^{\Xi}*D*}})_{trans} \approx 1$.

$$(\frac{Q_{C_3D_8}}{Q_{C_3H_8}})_{trans} = (\frac{m_{C_3D_8}}{m_{C_3H_8}})^{3/2} = 1.285$$

.

(2) Rotational partition function contribution:

$$\left(\frac{Q_{C_3D_8}}{Q_{C_3H_8}}\right)_{rot} = (\frac{(I_x I_y I_{z)C_3D_8}}{(I_x I_y I_{z)C_3H_8}})^{0.5} = (\frac{28.1 \times 80.7 \times 90.3}{16.9 \times 59.8 \times 67.5})^{0.5} = 1.733$$

The C_3H_7*H* and C_3D_7*D* are adsorbed species, therefore, $(\frac{Q_{C_3H_7^{\Xi}*H*}}{Q_{C_3D_7^{\Xi}*D*}})_{rot} \approx 1$.

(3) Vibrational partition function contribution:

When T < 1000K, $(\frac{Q_{C_3H_7^{\Xi}*H*}}{Q_{C_3D_7^{\Xi}*D*}})_{vib} \approx 1;\ (\frac{Q_{C_3D_8}}{Q_{C_3H_8}})_{vib} \approx 1$

(4) Electronic partition function contribution:

$$\left(\frac{Q_{C_3H_7^{\Xi}*H*}}{Q_{C_3D_7^{\Xi}*D*}}\right)_{elec} = e^{(E_{C_3H_7^{\Xi}*H*} - E_{C_3D_7^{\Xi}*D*})/RT}$$

$$\left(\frac{Q_{C_3D_8}}{Q_{C_3H_8}}\right)_{elec} = e^{(E_{C_3H_8} - E_{C_3D_8})/RT}$$

Combing above equations, the kinetic isotopic effect can be approximated as

$$KIE = 2.23e^{\left[\left(E_{C_3H_8} - E_{C_3H_7^{\Xi}*H*}\right) - \left(E_{C_3D_8} - E_{C_3D_7^{\Xi}*D*}\right)\right]/RT}$$

In which $\left(E_{C_3H_8} - E_{C_3H_7^{\Xi}*H*}\right)$ is the zero-point energy difference between C_3H_8 and the corresponding transition state species, while $\left(E_{C_3D_8} - E_{C_3D_7^{\Xi}*D*}\right)$ is the zero-point energy difference between C_3D_8 and the corresponding transition state species. The zero-point energy of the transition state species cannot be determined; however, comparing propane and the corresponding transition state, the main difference in energy is two full C-H bond in propane changes to partially formed C-Pt, H-Pt, and C-H bonds in the transition state. So that the $\left(E_{C_3H_8} - E_{C_3H_7^{\Xi}*H*}\right)$ and $\left(E_{C_3D_8} - E_{C_3D_7^{\Xi}*D*}\right)$ can be approximately expressed as

$$E_{C_3H_8} - E_{C_3H_7^{\Xi}*H*} \approx E_{C-H} - E_{C^{\Xi}-H} - E_{H^{\Xi}-Pt} - E_{C^{\Xi}-Pt}$$

$$E_{C_3D_8} - E_{C_3D_7^{\Xi}*D*} \approx E_{C-D} - E_{C^{\Xi}-D} - E_{D^{\Xi}-Pt} - E_{C^{\Xi}-Pt}$$

Therefore,

$$\begin{aligned}\left(E_{C_3H_8} - E_{C_3H_6^{\Xi}*H*}\right) - \left(E_{C_3H_8} - E_{C_3H_6^{\Xi}*H*}\right) &\approx \left(E_{C-H} - E_{C^{\Xi}-H} - E_{H^{\Xi}-Pt} - E_{C^{\Xi}-Pt}\right) - \left(E_{C-D} - E_{C^{\Xi}-D} - E_{D^{\Xi}-Pt} - E_{C^{\Xi}-Pt}\right) \\ &\approx 0.3\left(E_{C-H} - E_{C^{\Xi}-H} - E_{H^{\Xi}-Pt}\right)\end{aligned}$$

Thus,

$$KIE = 2.23e^{0.3\left(E_{C-H} - E_{C^{\Xi}-H} - E_{H^{\Xi}-Pt}\right)/RT} \quad \text{-----(1)}$$

Assuming that second C-H cleavage is the rate determine step, then the kinetic isotope effect (KIE) which is defined as the ratio of PDH reaction rates equals to

$$KIE = \left(\frac{K_{I,\ C_3H_8}}{K_{I,\ C_3D_8}}\right)\left(\frac{K_{II,\ C_3H_8}}{K_{II,\ C_3D_8}}\right)\left(\frac{k_{III,\ C_3H_7*}}{k_{III,\ C_3D_7*}}\right)$$

Each parenthesis in above equation is examined separately as follows.

$$\frac{K_{I,\ C_3H_8}}{K_{I,\ C_3D_8}} = \frac{\frac{Q_{C_3H_8*}}{Q_{C_3H_8}Q_*}}{\frac{Q_{C_3D_8*}}{Q_{C_3D_8}Q_*}}$$

$$\frac{K_{II,\ C_3H_8}}{K_{II,\ C_3D_8}} = \frac{\frac{Q_{C_3H_7*H*}}{Q_{C_3H_8}Q*}}{\frac{Q_{C_3D_7*D*}}{Q_{C_3D_8*}Q_*}}$$

$$\frac{k_{III,\ C_3H_7*}}{k_{III,\ C_3D_7*}} = \frac{\frac{Q_{C_3H_6^{\Xi}*H*}}{Q_{C_3H_7*}Q_*}}{\frac{Q_{C_3D_6^{\Xi}*D*}}{Q_{C_3D_7*}Q_*}}$$

Combing the above three equations results in

$$KIE = \frac{Q_{C_3H_6^{\Xi}*H*}Q_{C_3D_7*}Q_{C_3H_7^{\Xi}*H*}Q_{C_3D_8}}{Q_{C_3D_6^{\Xi}*D*}Q_{C_3H_7*}Q_{C_3D_7^{\Xi}*D*}Q_{C_3H_8}} \approx \frac{Q_{C_3H_6^{\Xi}*H*}Q_{C_3D_8}}{Q_{C_3D_6^{\Xi}*D*}Q_{C_3H_8}}$$

Each ratio of partition functions is evaluated as follows.

(1) Translational partition function contribution:

$$\left(\frac{Q_{C_3D_8}}{Q_{C_3H_8}}\right)_{trans} = \left(\frac{m_{C_3D_8}}{m_{C_3H_8}}\right)^{3/2} = 1.285$$

The C_3H_6*H* and C_3D_6*D* adsorbed species have zero translational degrees of freedom, and the reduce masses of C_3H_6*H* and C_3D_6*D* adsorbed species are approximately the same. Therefore,

$$\left(\frac{Q_{C_3H_6^{\Xi}*H*}}{Q_{C_3D_6^{\Xi}*D*}}\right)_{trans} \approx 1$$

(2) Rotational partition function contribution:

$$\left(\frac{Q_{C_3D_8}}{Q_{C_3H_8}}\right)_{rot} = \left(\frac{(I_xI_yI_z)_{C_3D_8}}{(I_xI_yI_z)_{C_3H_8}}\right)^{0.5} = \left(\frac{28.1 \times 80.7 \times 90.3}{16.9 \times 59.8 \times 67.5}\right)^{0.5} = 1.733$$

The C_3H_6*H* and C_3D_6*D* are adsorbed species, therefore, $\left(\frac{Q_{C_3H_6^{\Xi}*H*}}{Q_{C_3D_6^{\Xi}*D*}}\right)_{rot} \approx 1$.

(3) Vibrational partition function contribution:

When T < 1000K, $\left(\frac{Q_{C_3H_6^{\Xi}*H*}}{Q_{C_3D_6^{\Xi}*D*}}\right)_{vib} \approx 1;\ \left(\frac{Q_{C_3D_8}}{Q_{C_3H_8}}\right)_{vib} \approx 1$

(4) Electronic partition function contribution:

$$\left(\frac{Q_{C_3H_6^{\Xi}*H*}}{Q_{C_3D_6^{\Xi}*D*}}\right)_{elec} = e^{(E_{C_3D_6^{\Xi}*D*} - E_{C_3H_6^{\Xi}*H*})/RT}$$

$$\left(\frac{Q_{C_3D_8}}{Q_{C_3H_8}}\right)_{elec} = e^{(E_{C_3H_8} - E_{C_3D_8})/RT}$$

Combing above equations, the kinetic isotopic effect can be approximated as

$$KIE = 2.23e^{\left[\left(E_{C_3H_8} - E_{C_3H_6^{\Xi}*H*}\right) - \left(E_{C_3D_8} - E_{C_3D_6^{\Xi}*D*}\right)\right]/RT} = 2.23e^{(\Delta E_H - \Delta E_D)/RT}$$

In which $\left(E_{C_3H_8} - E_{C_3H_6^{\Xi}*H*}\right)$ is the zero-point energy difference between C_3H_8 and the corresponding transition state species, while $\left(E_{C_3D_8} - E_{C_3D_6^{\Xi}*D*}\right)$ is the zero-point energy difference between C_3D_8 and the corresponding transition state species. The zero-point energy of the transition state species cannot be determined; however, comparing propane and the corresponding transition state, the main difference in energy is two full C-H bond in propane changes to partially formed C-Pt, H-Pt, and C-H bonds in the transition state. So that the $\left(E_{C_3H_8} - E_{C_3H_6^{\Xi}*H*}\right)$ and $\left(E_{C_3D_8} - E_{C_3D_6^{\Xi}*D*}\right)$ can be approximately expressed as

$$E_{C_3H_8} - E_{C_3H_6{}^{\Xi}_{*H*}} \approx 2E_{C-H} - E_{C\,{}^{\Xi}_{-}\,H} - E_{H\,{}^{\Xi}_{-}\,Pt} - E_{C\,{}^{\Xi}_{-}\,Pt}$$

$$E_{C_3D_8} - E_{C_3D_6{}^{\Xi}_{*D*}} \approx 2E_{C-D} - E_{C\,{}^{\Xi}_{-}\,D} - E_{D\,{}^{\Xi}_{-}\,Pt} - E_{C\,{}^{\Xi}_{-}\,Pt}$$

Therefore,

$$\begin{aligned}\left(E_{C_3H_8} - E_{C_3H_6{}^{\Xi}_{*H*}}\right) - \left(E_{C_3H_8} - E_{C_3H_6{}^{\Xi}_{*H*}}\right) \\ \approx \left(2E_{C-H} - E_{C\,{}^{\Xi}_{-}\,H} - E_{H\,{}^{\Xi}_{-}\,Pt} - E_{C\,{}^{\Xi}_{-}\,Pt}\right) - \left(2E_{C-D} - E_{C\,{}^{\Xi}_{-}\,D} - E_{D\,{}^{\Xi}_{-}\,Pt} - E_{C\,{}^{\Xi}_{-}\,Pt}\right) \\ \approx 0.3\left(2E_{C-H} - E_{C\,{}^{\Xi}_{-}\,H} - E_{H\,{}^{\Xi}_{-}\,Pt}\right)\end{aligned}$$

Thus,

$$KIE = 2.23e^{0.3\left(2E_{C-H} - E_{C\,{}^{\Xi}_{-}\,H} - E_{H\,{}^{\Xi}_{-}\,Pt}\right)/RT} \qquad \text{-----(2)}$$

In which E_{C-H} is the energy of the C−H bond in propane and $E_{C\,{}^{\Xi}_{-}\,H}$ and $E_{H\,{}^{\Xi}_{-}\,Pt}$ are the energies of partially formed C−H and H−Pt bonds in the transition state, respectively.

A normal kinetic isotope effect (rH /rD) of 1.65 and 2.39 have been found on the PtSn3Ca5/Al_2O_3 and PtSn3/Al_2O_3 catalysts *via* experiment, respectively. The different KIE indicating the different RDS on two above catalysts. The kinetic study in the present work has demonstrated that the reactor order of H_2 over PtSn3Ca5/Al_2O_3 is the first C-H cleavage. Therefore, the equation (1) was employed to calculate the sum of $E_{C\,{}^{\Xi}_{-}\,H}$ and $E_{H\,{}^{\Xi}_{-}\,Pt}$, which is 23.0 kJ. If the two catalysts share the same reaction mechanism, the energy can be employed for the calculation of theoretical KIE when second C-H is the RDS [23]. This gives a value of 3.25 for KIE over PtSn3/Al_2O_3, which is different with the 2.39 obtained from experiments. Thus, the change in KIE confirms the result obtained from kinetic analysis that neither the first C−H bond activation nor the second C−H bond activation is the RDS on PtSn3/Al_2O_3, which is consistent with the literatures that RDS for Pt-Sn catalysts relates to the composition of the surface[25].

References:

[1] J. P. Perdew, K. Burke, M. Ernzerhof, *Phys. Rev. Lett.* **1996**, *77*, 3865–3868.
[2] G. Kresse, J. Furthmüller, *Phys. Rev. B* **1996**, *54*, 11169–11186.
[3] G. Henkelman, B. P. Uberuaga, H. Jónsson, *The Journal of Chemical Physics* **2000**, *113*, 9901–9904.
[4] G. Henkelman, H. Jónsson, *The Journal of Chemical Physics* **1999**, *111*, 7010–7022.
[5] Y.-L. Shan, T. Wang, Z.-J. Sui, Y.-A. Zhu, X.-G. Zhou, *Catalysis Communications* **2016**, *84*, 85–88.
[6] Y. Zhang, Y. Zhou, J. Shi, S. Zhou, X. Sheng, Z. Zhang, S. Xiang, *Journal of Molecular Catalysis A: Chemical* **2014**, *381*, 138–147.
[7] L. Shi, G.-M. Deng, W.-C. Li, S. Miao, Q.-N. Wang, W. Zhang, W. Zhang, An-Hui Lu, A.-H. Lu, *Angewandte Chemie* **2015**, *54*, 13994–13998.
[8] C. Sun, J. Luo, M. Cao, P. Zheng, G. Li, J. Bu, Z. Cao, S. Chen, X. Xie, *Journal of Energy Chemistry* **2018**, *27*, 311–318.
[9] H. Zhu, D. H. Anjum, Q. Wang, E. Abou-Hamad, L. Emsley, H. Dong, P. Laveille, L. Li, A. K. Samal, J.-M. Basset, *Journal of Catalysis* **2014**, *320*, 52–62.
[10] O. A. Bariås, A. Holmen, E. A. Blekkan, *Journal of Catalysis* **1996**, *158*, 1–12.
[11] Y. Duan, Y. Zhou, Y. Zhang, X. Sheng, M. Xue, *Catal Lett* **2011**, *141*, 120–127.
[12] H. Zhang, Y. Zhang, Y. Zhou, X. Sheng, C. Zhang, J. Fang, S. Zhao, Y. Gao, *New Journal of Chemistry* **2018**, *42*, 103–110.
[13] J. Salmones, J.-A. Wang, J. A. Galicia, G. Aguilar-Rios, *Journal of Molecular Catalysis A: Chemical* **2002**, *184*, 203–213.
[14] Y. Zhu, Z. An, H. Song, X. Xiang, W. Yan, J. He, *ACS Catal.* **2017**, *7*, 6973–6978.
[15] S. Rimaz, L. Chen, A. Monzón, S. Kawi, A. Borgna, *Chemical Engineering Journal* **2021**, *405*, 126656.
[16] L. Qi, M. Babucci, Y. Zhang, A. Lund, L. Liu, J. Li, Y. Chen, A. S. Hoffman, S. R. Bare, Y. Han, B. C. Gates, A. T. Bell, *J. Am. Chem. Soc.* **2021**, *143*, 21364–21378.
[17] L. Liu, M. López-Haro, C. W. Lopes, S. Rojas-Buzo, P. Concepción, R. Manzorro, L. Simonelli, A. Sattler, P. Serna, Pedro Serna, J. J. Calvino, A. Corma, *Nature Catalysis* **2020**, *3*, 628–638.
[18] L. Liu, M. López-Haro, C. W. Lopes, C. Li, P. Concepción, L. Simonelli, J. J. Calvino, A. Corma, *Nature Materials* **2019**, *18*, 866–873.
[19] R. Qin, K. Liu, Q. Wu, N. Zheng, *Chem. Rev.* **2020**, *120*, 11810–11899.
[20] J. H. Kwak, J. Hu, D. Mei, C. W. Yi, D. H. Kim, C. H. F. Peden, L. F. Allard, J. Szanyi, *Science* **2009**, *325*, 1670–1673.
[21] Z. Zhang, Y. Zhu, H. Asakura, B. Zhang, J. Zhang, M. Zhou, Y. Han, T. Tanaka, A. Wang, T. Zhang, N. Yan, *Nat Commun* **2017**, *8*, 16100.
[22] L. Wang, T. Maxisch, G. Ceder, *Phys. Rev. B* **2006**, *73*, 195107.
[23] J. Zhu, M.-L. Yang, Y. Yu, Y.-A. Zhu, Z.-J. Sui, X.-G. Zhou, A. Holmen, D. Chen, *ACS Catalysis* **2015**, *5*, 6310–6319.
[24] K. Chen, E. Iglesia, A. T. Bell, *Journal of Catalysis* **2000**, *192*, 197–203
[25] C. H. Fricke, O. H. Bamidele, M. Bello, J. Chowdhury, G. Terejanu, A. Heyden, *ACS Catal.* **2023**, *13*, 10627–10640.